Journal of Power Sources 195 (2010) 877–882

Contents lists available at ScienceDirect

Journal of Power Sources

journal homepage: www.elsevier.com/locate/jpowsour

Short communication

Differential voltage analyses of high-power lithium-ion cells. 4. Cells containing NMC☆

Ira Bloom[a,*], Lee K. Walker[a], John K. Basco[a], Daniel P. Abraham[a], Jon P. Christophersen[b], Chinh D. Ho[b]

[a] Argonne National Laboratory, 9700 South Cass Avenue, Argonne, IL 60439, USA
[b] Idaho National Laboratory, P.O. Box 1625, Idaho Falls, ID 83415, USA

ARTICLE INFO

Article history:
Received 22 June 2009
Received in revised form 3 August 2009
Accepted 10 August 2009
Available online 18 August 2009

Keywords:
Lithium-ion battery
Capacity fade
Battery testing

ABSTRACT

Cells with and without a $LiC_2O_4BF_2$ electrolyte additive and that contained $Li_{1.05}(Mn_{1/3}Co_{1/3}Ni_{1/3})_{0.95}O_2$ (NMC) positive electrodes were tested for calendar and cycle life at 60% state of charge. The temperatures used in these tests were 25 and 45 °C (cycle life) and 45 and 55 °C (calendar life). An analysis of the C/25 capacity data shows that the C/25 capacity decreases with the square root of time. The additive slowed down the rate of capacity decline.

The C/25 data were subjected to differential voltage analysis to determine the possible cause of the capacity decrease and at which electrode the capacity decrease was occurring. Data from full cells and half-cells were compared to elucidate individual electrode contributions. This analysis indicated that lithium-capacity-consuming side reactions were occurring primarily at the negative electrode.

1. Introduction

Lithium-ion batteries continue to attract much interest in applications where high specific or volumetric power or energy is required. High-power lithium-ion batteries are also being considered for automotive applications by the U.S. Department of Energy-supported Freedom Cooperative Automotive Research (FreedomCAR) Partnership [1]. The batteries usually consist of a metal-oxide positive electrode, a carbon negative electrode, and an organic electrolyte containing dissolved lithium salts.

Two national laboratories, Argonne National Laboratory (ANL) and Idaho National Laboratory (INL), continue to collaborate to understand the causes of performance declines in lithium-ion batteries. Previous results from this collaboration using two positive electrode materials, $LiNi_{0.8}Co_{0.2}O_2$ and $LiNi_{0.8}Co_{0.1}Al_{0.1}O_2$ (NCA), have been presented earlier [2–7]. Recently, the study was extended to include cells containing $Li_{1.05}(Mn_{1/3}Co_{1/3}Ni_{1/3})_{0.95}O_2$ (NMC) positive electrodes. These cells were aged according to the procedures described in an earlier paper [2]. NMC has been reported to have superior aging characteristics over the other materials that were studied [8–12].

The cells were characterized in terms of many parameters, including C/25 capacity measurements. These data were then analyzed in terms of their time dependence and by differential voltage (dV/dQ) analysis to elucidate some of the capacity fade mechanisms in the cells. The derivative of voltage with respect to capacity, dV/dQ, is well suited for graphical analysis of battery data, since the voltage of a cell can be written as

$$V_{cell} = V_{cathode} - V_{anode},$$

$(dV/dQ)_{cell}$ can be written as

$$\left(\frac{dV}{dQ}\right)_{cell} = \left(\frac{dV}{dQ}\right)_{cathode} - \left(\frac{dV}{dQ}\right)_{anode}.$$

That is, the contributions from the anode and cathode electrodes add linearly. This contrasts to the way the contributions add when using dQ/dV,

$$\frac{dQ}{dV_{cell}} = \frac{1}{(dV/dQ)_{cathode} - (dV/dQ)_{anode}}.$$

In a dV/dQ curve, the peaks are from phase transitions, whereas the peaks in a dQ/dV curve are from phase equilibria. At equilibrium, two or more coexisting phases have the same lithium chemical potential. Thus, $dV = 0$ at equilibrium, making dQ/dV undefined. On the other hand, dQ is never zero using a constant-current discharge or charge.

The peaks in the dV/dQ curves were assigned to the positive electrode, to the negative electrode, or to their sum by compari-

☆ The submitted manuscript has been created by UChicago Argonne, LLC, Operator of Argonne National Laboratory ("Argonne"). Argonne, a U.S. Department of Energy Office of Science laboratory, is operated under Contract No. DE-AC02-06CH11357. The U.S. Government retains for itself, and others acting on its behalf, a paid-up, non-exclusive, irrevocable, worldwide license in said article to reproduce, prepare derivative works, distribute copies to the public, and perform publicly and display publicly, by or on behalf of the Government.

* Corresponding author. Tel.: +1 630 252 4516; fax: +1 630 252 4176.
E-mail address: ira.bloom@anl.gov (I. Bloom).

0378-7753/$ – see front matter © 2009 Elsevier B.V. All rights reserved.
doi:10.1016/j.jpowsour.2009.08.019

son with half-cell data. In the work that follows, we continue the discussion of the technique and show how to use dV/dQ analysis in a case where side reactions occur at the negative electrode. Evidence of these reactions was seen in both calendar- and cycle-life experiments.

2. Experimental

2.1. Pouch cells

Two types of pouch cells, baseline and additive, were constructed according to ANL's specifications. The baseline cell chemistry is given in Table 1. The additive cells contain 2 wt% $LiC_2O_4BF_2$ in the electrolyte. The rated C/1 capacity for these cells was 0.4 Ah. The average electrode active area in each case was 377 cm^2. Details of pouch cell construction are given in Table 2.

The test matrix is given in Table 3, and the cells were aged as described in Ref. [2]. Briefly, the cells were characterized in terms of their charge and discharge C/25 capacities, in terms of their C/1 capacities and in terms of their power characteristics using the hybrid pulse power characterization test (HPPC) at 25 °C before the test began. The cells were then aged under calendar- or cycle-life profiles. The calendar-life cells were aged at 45 and 55 °C; the cycle-life cells, 25 and 45 °C. The state of charge (SOC) for these tests was 60% (3.70 V). After 4 weeks at the test temperature, the cells were cooled to 25 °C and reference performance tests were performed. The reference performance tests included C/25 capacity measurements. The cells were then heated back to the test temperature. This process was repeated for a maximum of 64 weeks. It should be noted that the baseline cells were tested for only calendar life at the two temperatures. Three baseline cells were tested at 45 °C and two at 55 °C. More details are given in Refs. [2,13].

Table 1
Cell chemistry.

Component	Composition
Negative electrode	90% MCMB 10-28 2% VGCF 8% PVDF Binder (KF1100) Loading density: 6.5 mg cm^{-2} 18 μm Cu foil Electrode coating thickness: 51 μm
Positive electrode	84% Seimi L-333 ($Li_{1.05}(Mn_{1/3}Co_{1/3}Ni_{1/3})_{0.95}O_2$) 8% SuperP carbon black 8% PVDF binder (KF7208) Loading density: 10.2 mg cm^{-2} L-333 20 μm Al foil Electrode coating thickness: 51 μm
Electrolyte	1.2 M $LiPF_6$ in EC:EMC (3:7 by wt)
Separator	25 μm

Table 2
Pouch cell construction.

Cell dimensions	Width: 35.0 mm Length: 62.0 mm
Electrode dimensions	Cathode(+) width: 30.5 mm Cathode(+) length: 51.5 mm Cathode(+) thickness: 120 μm Anode(−) width: 31.5 mm Anode(−) length: 53.0 mm Anode(−) thickness: 117.0 μm
Stack	Cathode/anode: 12 sheets/13 sheets
Tabs	Anode: nickel (mm·μm): 7 × 100 Cathode: aluminum (mm·μm): 7 × 100

Table 3
Test matrix for the additive cells.

Test	Temperature, °C	Cell count
Cycle life	25	5
	45	4
Calendar life	45	5
	55	5

2.2. Half-cells

Small sections of the positive and negative electrodes from fresh cells were assembled into button cells. Details of coin cell preparation are given in Ref. [7]. The half-cells consisted of 1.6-cm^2 sections of the electrode, new separator material, fresh electrolyte, and excess lithium foil. After assembly, the button cells were cycled at room temperature between 3 and 4.3 V for the positive and ~5 mV and 1.5 V for the negative. The charge and discharge rates were C/42 for the positive material and C/170 for the negative material. The charge and discharge voltages were measured and recorded at variable rates. If the voltage change was greater or equal to 10 mV, the data were recorded. Otherwise, data were recorded every 5 min for the positive and every 60 min for the negative. This procedure yielded about 300–500 points for further analysis.

2.3. Data reduction and calculations

The C/25 capacity values from each test condition were averaged and plotted vs. time and temperature. Approximations to the average kinetic law for C/25 capacity fade were obtained by using the LINEST function in Microsoft Excel®.

As described in Ref. [3], the capacity and voltage values from the C/25 discharges were subjected to mathematical filtering to average out the noise and accentuate the peaks. The filtering produced 200 points for subsequent manipulation and plotting. $-Q_o dV/dQ$ (hereafter referred to as dV/dQ) was calculated as $-Q_o \times \Delta V/\Delta(\text{Ah})$, where Q_o is the measured C/25 capacity of the cell, in Ah; $\Delta(\text{Ah})$ is the change in the capacity of the cell in a given interval; and ΔV is the change in cell voltage as a result of $\Delta(\text{Ah})$. The $-Q_o$ factor served to normalize the derivatives based on cell capacity. Further smoothing of the dV/dQ curve was accomplished by using a 5-point moving average. Plots of dV/dQ vs. capacity density (mAh cm^{-2}) were then analyzed for trends in peak position and pattern. No mathematical changes were made to the negative-to-positive ratio.

Peaks were assigned by comparing the dV/dQ curve of the cell to those from the half-cells. Estimations of the C/25 discharge curve and the dV/dQ curve were made by shifting the positive electrode data from the half-cells relative to the data from the negative electrode. For these C/25 curve estimations, the full-cell potentials were calculated by subtracting the potential of the negative electrode from that of the positive electrode. The cell capacity was defined as that between the voltage limits of 4.0 and 3.0 V.

3. Results

A representative C/1 discharge curve is shown in Fig. 1a and how the C/1 capacity changes with time is shown in Fig. 1b. The curves display the features typical of using a layered material cathode and a graphite anode. As expected, the C/1 capacity decreased as the cells aged at all temperatures. The corresponding available power and energy curves calculated from the HPPC test, are given in Fig. 2. Fig. 2 also shows declining power and energy as a function of time. This manuscript, however, is limited to just the C/25 data, how they change with time and analysis of these data.

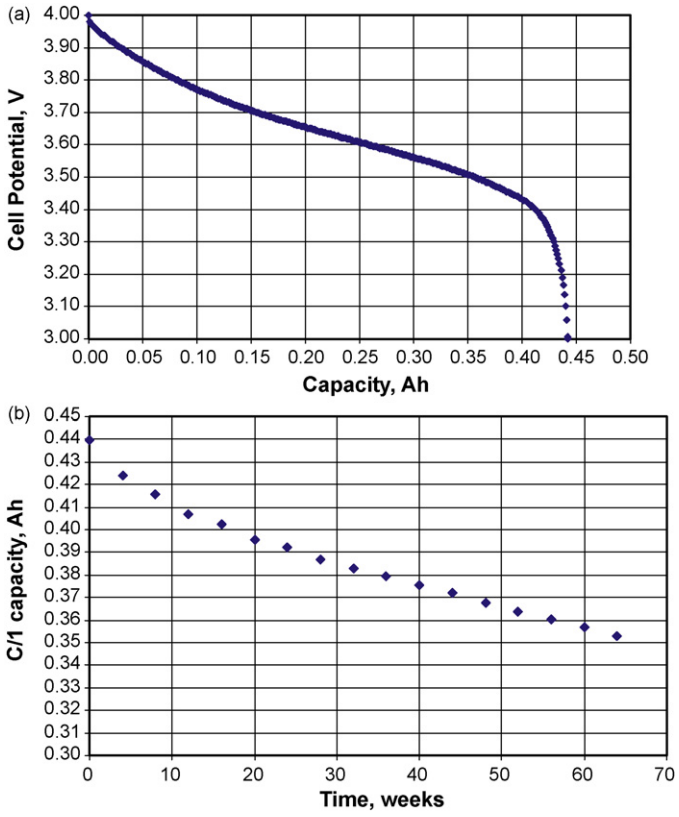

Fig. 1. (a) Typical C/1 discharge curve at characterization. (b) Typical C/1 capacity vs. time from an additive cell that was cycled at 45 °C. The C/1 capacity was measured at 30 °C.

3.1. C/25 capacity fade

The initial average C/25 capacity values 0.480 and 0.466 Ah were found for the baseline and additive pouch cells, respectively. As expected, the C/25 capacity decreased as the cells aged at all temperatures. C/25 discharge curves from a typical additive cell are given in Fig. 3 for a calendar-life pouch cell.

Plotting the C/25 capacity data vs. time produces Fig. 4. From Fig. 4, the effect of temperature on the C/25 data can clearly be seen. The relative capacity decline increases with test temperature. Fig. 2 also shows that the rate of relative C/25 capacity decline in the

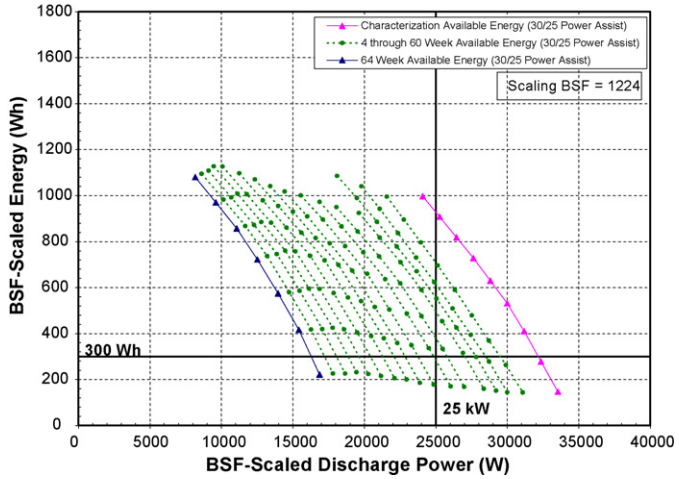

Fig. 2. Available energy vs. power as a function of time. The time between RPTs is 4 weeks.

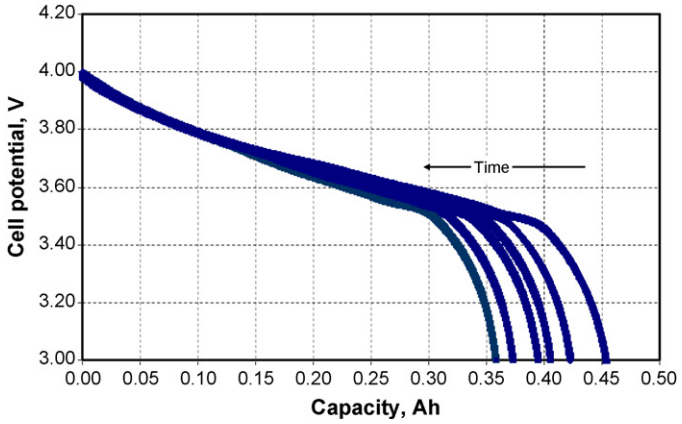

Fig. 3. Cell potential vs. capacity from C/25 discharge curves from a typical additive cell. The time between curves is 4 weeks.

baseline cells is higher than those seen in the additive cells. Thus, the $LiC_2O_4BF_2$ additive appears to retard C/25 capacity fade. There also seems to be test dependence at 45 °C for the NMC material, with the calendar-life cells fading faster than the cycle-life cells.

The data shown in Fig. 4 were then subjected to least-squares fitting, assuming parabolic, diffusion-controlled kinetics, $C = z + kt^{1/2}$, where C is the relative capacity, z is the initial capacity (ideally = 1), k is the rate constant, and t is time in weeks. These results are shown in Table 4 along with the regression coefficient, r^2. Fig. 4 also shows the resulting curves from the fitting. From these data, the fit is very good.

Examining the values of k in Table 4 shows the expected trends. The magnitude of k increases with temperature in both types of cells. The magnitude of k is also greater in the baseline cells than in the corresponding additive cells; the average fade rate in the baseline cells is greater than that in the additive cells. From a practical standpoint, the C/25 capacity fade rates are approximately the same and the same as those found from the NCA-containing cells [3].

3.2. Differential voltage analysis

Plots of typical dV/dQ vs. capacity density curves at $t = 0$ are shown in Fig. 5 for both the baseline and additive cells. Fig. 5 shows that the dV/dQ vs. capacity density curves from the two types of

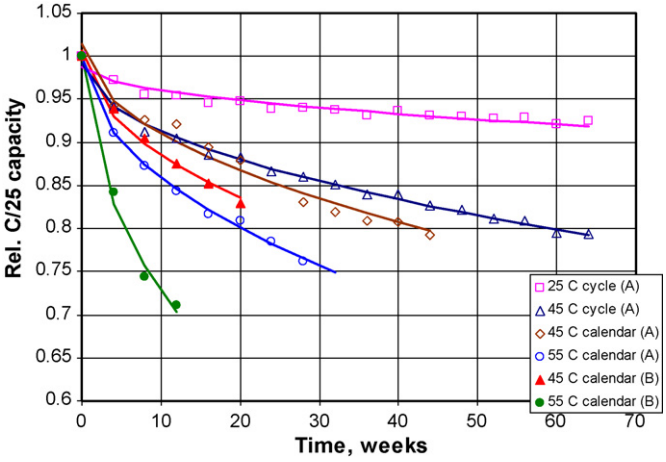

Fig. 4. Relative C/25 capacity for the cells under test as a function of composition, temperature, and time. The symbols are the data points, and the solid lines represent the least-squares fit to the data. The notation (A) in the legend signifies additive cells and (B), baseline cells.

Table 4
Results from least-squares fitting using the C/25 data.

Test matrix condition/cell type	z, Ah (std. error)	k, Ah/week (std. error)	r^2
Calendar life at 45 °C/baseline	1.00 (6.41×10^{-3})	-3.83×10^{-2} (2.03×10^{-3})	0.99
Calendar life at 55 °C/baseline	1.00 (1.38×10^{-2})	-8.58×10^{-2} (2.03×10^{-3})	0.99
Cycle life at 25 °C/additive	0.99 (3.42×10^{-3})	-8.59×10^{-3} (6.04×10^{-4})	0.93
Cycle life at 45 °C/additive	0.99 (2.70×10^{-4})	-2.50×10^{-2} (4.76×10^{-4})	0.99
Calendar life at 45 °C/additive	1.01 (8.41×10^{-3})	-3.27×10^{-2} (1.80×10^{-3})	0.96
Calendar life at 55 °C/additive	1.00 (3.30×10^{-3})	-4.42×10^{-2} (8.90×10^{-4})	0.99

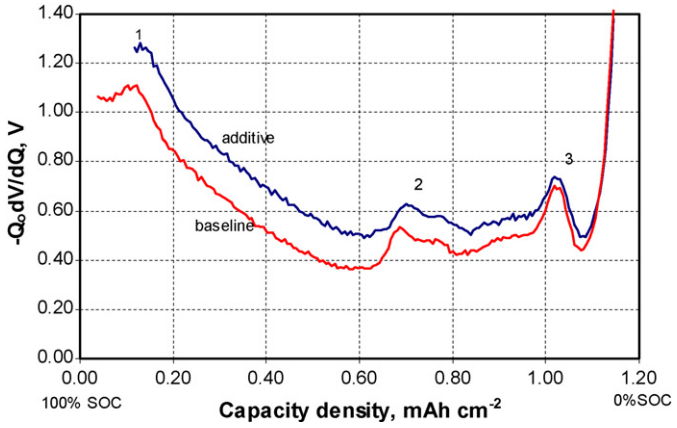

Fig. 5. $-Q_o dV/dQ$ vs. capacity density curves from typical baseline and additive pouch cells. The SOC vs. capacity density convention used in this figure is implicit for the rest in this paper.

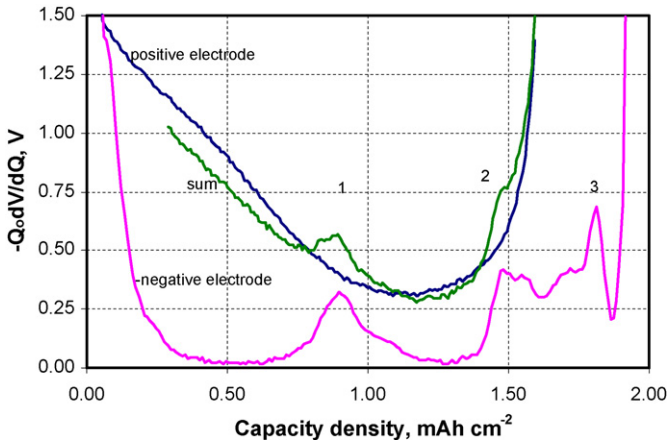

Fig. 6. $-Q_o dV/dQ$ vs. capacity density curves from half-cell data and their sum, assuming perfect electrode alignment and a voltage range of 3.0–4.0 V.

cells are essentially the same in terms of the visible peaks. Thus, the additive does not appear to affect the dV/dQ vs. capacity density curves. The difference between the curves at high SOC is due to electrode alignment or "slippage" [3]. As used here, the terms electrode alignment and "slippage" denote the capacity density difference of the electrochemically active sections of the anode and the cathode which define the potential window. The effect of slippage on the dV/dQ curve is discussed in detail below. The amount of slippage directly affects the position and width of voltage window of the electrode that is used during battery cycling.

Slippage arises due to the loss of lithium capacity while maintaining the cell voltage limits. The capacity decline can be from actual damage of the electrode material or the loss of the more-reactive portions of the electrode due to the product of a side reaction blocking it. The apparent slippage arises from these types of phenomena occurring faster on one electrode than the other.

The peaks in Fig. 5 were assigned to electrodes by comparison with dV/dQ curves from half-cells (Fig. 6), assuming perfect electrode alignment (i.e., 0.0 mAh cm^{-2} slippage) and an operating voltage range of 3.0–4.0 V. Comparing Figs. 3 and 4 shows that the peaks in the sum are from the negative electrode. The dV/dQ curve from the positive electrode material is featureless, indicating that there are no first-order phase transitions.

However, the sum of the dV/dQ curves from the two half-cells using a slippage value of 0.0 mAh cm^{-2} does not accurately represent the finer details shown in Fig. 5. For example, the tail at high SOC before peak 1 in Fig. 6 is much shorter than that in Fig. 5 in the baseline cell and does not exist at all in the additive cell. The dV/dQ curve for the additive cell starts at almost the apex of peak 1.

A better approximation of Fig. 6 was obtained by increasing the electrode slippage value. Fig. 7 shows the effect on the dV/dQ curve when the amount of electrode slippage is increased from 0.500 to 0.875 mAh cm^{-2}. From these results, electrode slippage values of 0.500 and 0.625 mAh cm^{-2} produce dV/dQ curves that approximate those from the baseline and additive cells, respectively.

Since the peaks have been assigned and the initial dV/dQ curve approximated, let us now analyze the dV/dQ data given in Fig. 8a and b to determine if the source of the capacity fade can be identified. For this analysis, the source of capacity fade will be thought of as arising from two root causes: the loss of accessible active material or the change in the alignment of the electrodes due to side reactions. The latter source is the same as the adjustments that were made to align the half-cell data with those from the pouch cell.

Comparing the curves shown in Fig. 8a with those shown in Fig. 7 shows that they follow a similar pattern. In Fig. 8, peak 1 disappears with aging time. In Fig. 7, starting from an initial value of electrode slippage, peak 1 tends to disappear as positive electrode slippage

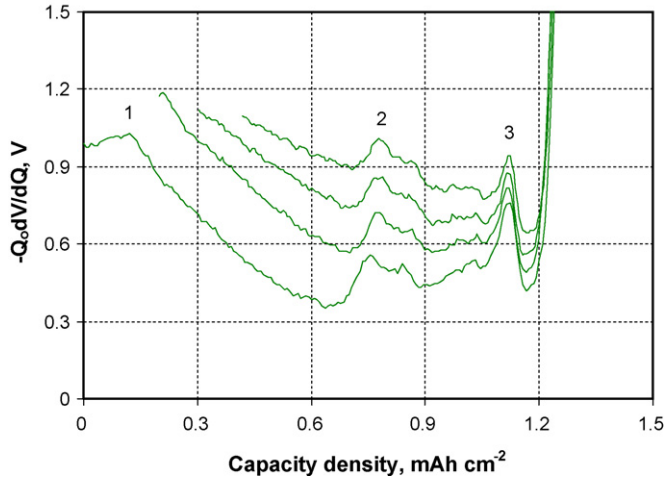

Fig. 7. Calculated $-Q_o dV/dQ$ vs. capacity density as a function of electrode slippage at the positive electrode, based on half-cell data. The bottommost curve represents 0.500 mAh cm^{-2} slippage, and the topmost, 0.875 mAh cm^{-2}. The slippage increment between each curve is 0.125 mAh cm^{-2}. These curves have been horizontally translated after the dV/dQ calculation so that peak 3 aligns. Also, a vertical translation has been added for the sake of clarity.

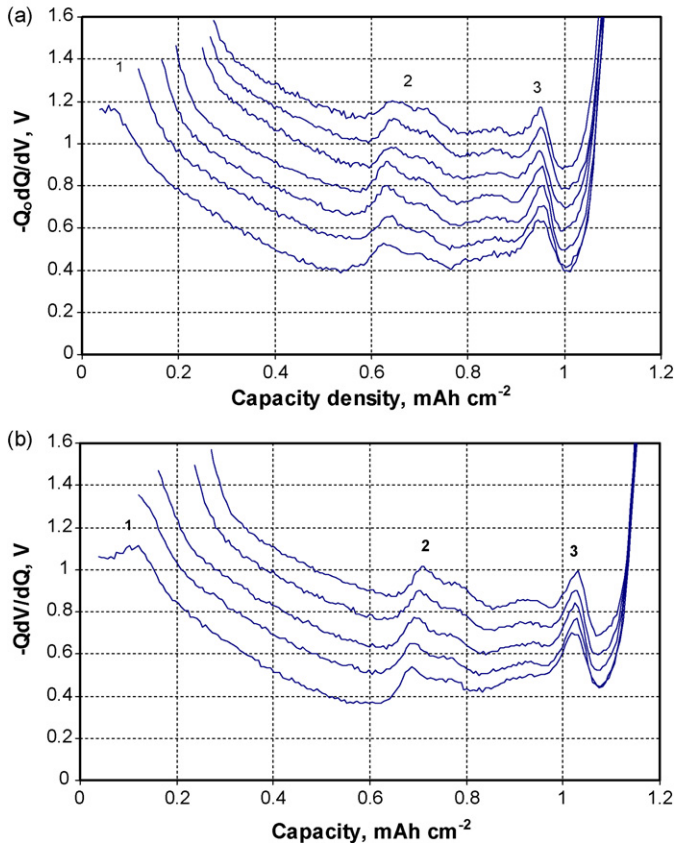

Fig. 8. (a) $-Q_o dV/dQ$ vs. capacity density curves from an additive pouch cell. Time increases vertically. A vertical offset was added for the sake of clarity and the curves were offset horizontally so that peak 3 aligns in each curve. The time difference between curves is 4 weeks. (b) $-Q_o dV/dQ$ vs. capacity density curves from a baseline cell. Time increases vertically. A vertical offset was added for the sake of clarity. The curves were also offset horizontally so that peak 3 aligns in each curve.

increases. The same observations can be made by comparing the curves in Fig. 7b with those in Fig. 7.

As a point of contrast, if the negative electrode were shifting, the changes in the peak pattern would be very different. This is shown in Fig. 9. Here, peaks 2 and 3 vanish with increasing electrode slippage.

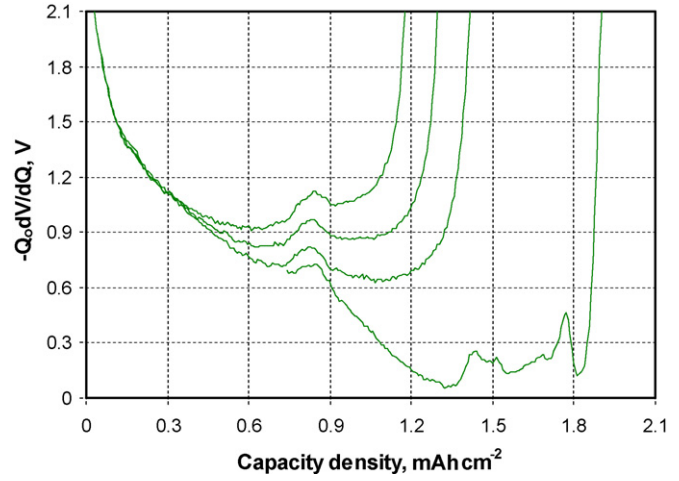

Fig. 9. Calculated $-Q_o dV/dQ$ vs. capacity density for a full cell, based on half-cell data, as a function of negative electrode slippage. The bottommost curve represents the $t = 0$ condition (slippage = 0.5 mAh cm^{-2}). Slippage increases at the negative electrode from 0 to 0.375 mAh cm^{-2} vertically. The change in slippage between each curve is 0.125 mAh cm^{-2}. These curves have been horizontally translated after the dV/dQ calculation so that peak 1 aligns. Also, a vertical translation has been added for the sake of clarity.

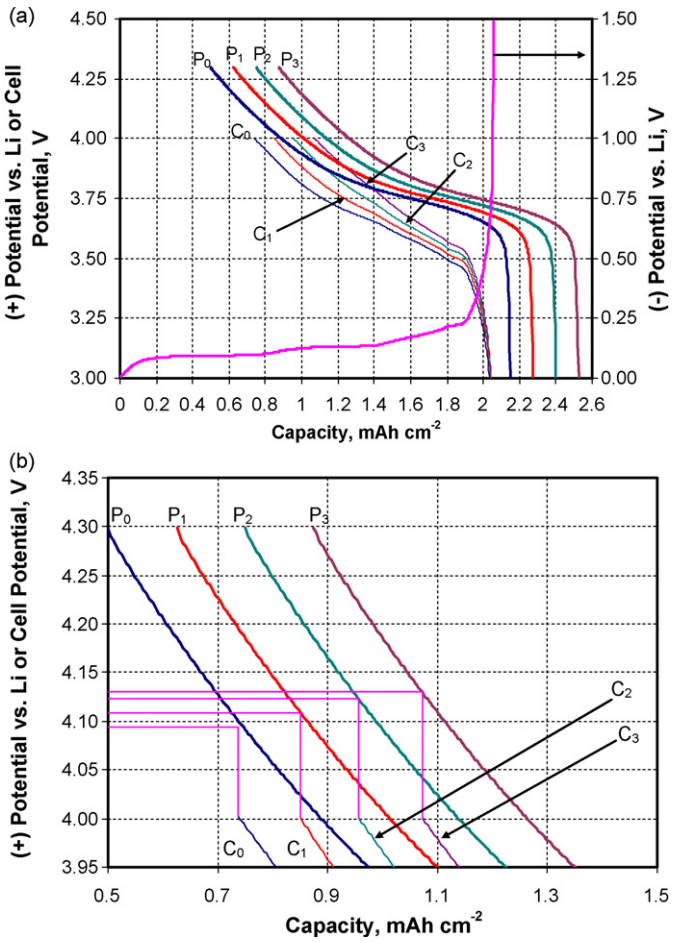

Fig. 10. (a) Schematic of cell potential vs. capacity density showing the effect of positive electrode shifting on the active operating voltage window, assuming voltage limits of 4.0 and 3.0 V. The curves marked P_n, where $n = 0$, 1, 2, and 3, represent the voltage vs. capacity density curves of the positive electrode using different slippage values. The amount of slippage for P_0 is 0.500 mAh cm^{-2} and for P_3, 0.875 mAh cm^{-2}. The curves marked C_n represent the operating cell voltage curves using the nth positive electrode curve. (b) Enlargement of the cell high-potential region shown in Fig. 8a, showing that, as slippage increases, higher potential regions of the positive become involved in the cell discharge and charge reactions. The horizontal and vertical lines were added to aid the eye. In this figure, the 4.000-V cell potential corresponds to 4.094, 4.109, 4.123, and 4.130 V on P_0, P_1, P_2, and P_3, respectively.

4. Discussion

The apparent loss of C/25 capacity can be due to many factors, such as side reactions. These side reactions may lead to solid electrolyte interface (SEI) layer growth or simply removal of active lithium from the cell. Sample reactions are given in Refs. [13–19]. However, the data up to this point do not reveal which electrode is the primary location of observed C/25 capacity loss.

Analysis of the dV/dQ curves can be used to determine which electrode is the major source of capacity fade and what type of reaction is occurring. From the data shown in Figs. 7, 8a and b, shifts in the alignment of the electrodes due to side reactions seems to be the primary cause of capacity fade, and it is the positive electrode that is shifting.

Fig. 10a shows schematically the effect of positive electrode shifting on the available capacity of the cell. Here, the voltage limits were kept constant at 4.0 and 3.0 V. As the amount of shift of the positive increases (the curves marked P_n in Fig. 10a), the resulting

calculated cell voltage vs. capacity density curves (denoted as C_n in Fig. 10a) also shift correspondingly. During this shifting process, higher potential portions of the positive electrode, which were previously not used, now become an active part of the cell discharge and charge reactions, as shown in Fig. 10b. At the same time, for the voltage limits of 4.0 and 3.0 V, the available capacity decreases as the shift increases.

In other words, as the side reactions proceed, the lower potential regions of the negative electrode would be effectively removed from the active electrochemistry and, thus, charging the cell would terminate, incompletely lithiating the negative electrode. Compared to its starting point, the negative electrode is now at a higher potential. To maintain a 4.0 V limit, there would be a compensatory shift at the positive electrode to higher potentials. From this starting point, discharge would similarly end at different degrees of lithiation/delithiation for the two electrodes, as compared their starting points, to maintain the 3.0 V lower voltage limit.

Comparing these results to those obtained using NCA positives [3,18] shows that these electrode-shifting reactions occurred at the negative electrode. Both NCA- and NMC-containing cells consisted of a layered-oxide positive and a graphite-based negative. Even though the negative electrodes were different materials (MAG10 vs. MCB), the basic phenomenology did not change.

5. Conclusion

Cells with and without a $LiC_2O_4BF_2$ additive and that contained NMC positives were tested for calendar and cycle life at 60% SOC. The temperatures used in these tests were 25 and 45 °C (cycle life) and 45 and 55 °C (calendar life). An analysis of the C/25 capacity data shows that the C/25 capacity decreases with the square root of time. The additive slowed down the rate of capacity decline. At 55 °C, the rate of capacity decline decreased by about a factor of 2.

The C/25 data were subjected to dV/dQ analysis to determine the possible cause of the capacity decrease and at which electrode the capacity decrease was occurring. The analysis indicated that lithium-capacity-consuming side reactions were occurring primarily at the negative electrode, which was similar to what was seen in cells containing NCA.

Acknowledgment

This work was performed under the auspices of the U.S. Department of Energy, Office of Vehicle Technologies, Hybrid and Electric Systems, under Contract No. DE-AC02-06CH11357 (ANL) and under Contract No. DE-AC07-99ID13727 (INL).

References

[1] FY2008 Progress Report for Energy Storage Research and Development, U.S. Department of Energy, January 2009. http://www1.eere.energy.gov/vehiclesandfuels/pdfs/program/2008_energy_storage.pdf.
[2] I. Bloom, S.A. Jones, V.S. Battaglia, G.L. Henriksen, J.P. Christophersen, R.B. Wright, C.D. Ho, J.R. Belt, C.G. Motloch, J. Power Sources 124 (2003) 538.
[3] I. Bloom, A.N. Jansen, D.P. Abraham, J. Knuth, S.A. Jones, V.S. Battaglia, G.L. Henriksen, J. Power Sources 139 (2005) 295.
[4] I. Bloom, J. Christophersen, K. Gering, J. Power Sources 139 (2005) 304.
[5] I. Bloom, B.G. Potter, C.S. Johnson, K.L. Gering, J.P. Christophersen, J. Power Sources 155 (2006) 415.
[6] I. Bloom, J.P. Christophersen, D.P. Abraham, K.L. Gering, J. Power Sources 157 (2006) 537.
[7] D.P. Abraham, J.L. Knuth, D.W. Dees, I. Bloom, J.P. Christophersen, J. Power Sources 170 (2007) 465.
[8] N. Yabuuchi, T. Ohzuku, J. Power Sources 119–121 (2003) 171.
[9] H. Yoshizawa, T. Ohzuku, J. Power Sources 174 (2007) 813, and references cited therein.
[10] N. Yabuuchi, Y. Makimura, T. Ohzuku, J. Power Sources 154 (2007) A314.
[11] S. Cordova, Z. Johnson, K.M. Abraham, Proceedings from the 43rd Power Sources Conference, July, 2008, p. 307.
[12] S. Ferguson, D. Kelley, S. Gargies, Proceedings from the 43rd Power Sources Conference, July, 2008, p. 461.
[13] PNGV Battery Test Manual, DOE/ID-10597, Rev. 3, U.S. Department of Energy, February 2001.
[14] A.M. Andersson, D.P. Abraham, R. Haasch, S. MacLaren, J. Liu, K. Amine, J. Electrochem. Soc. 149 (2002) A1358.
[15] D. Ensling, M. Stjerndahl, A. Nytén, T. Gustafsson, J.O. Thomas, J. Mater. Chem. 19 (2009) 82.
[16] P. Arora, R.E. White, M. Doyle, J. Electrochem. Soc. 145 (1998) 3647.
[17] D. Aurbach, B. Markovsky, M.D. Levi, E. Levi, A. Schechter, M. Moshkovich, Y. Cohen, J. Power Sources 81/82 (1999) 95.
[18] D.P. Abraham, S.D. Poppen, A.N. Jansen, J. Liu, D.W. Dees, Electrochim. Acta 49 (2004) 4763.
[19] A. Xiao, L. Yang, B.L. Lucht, S.-H. Kang, D.P. Abraham, J. Electrochem. Soc. 156 (2009) A318.